scientific reports

Check for updates

OPEN

# Uricase-free and cost-effective colorimetric assay for uric acid based on CoBTC metal–organic frameworks

Shokooh Sadat Khaloo[1,2]✉, Mohammad Hossein Vaziri[1,2] & Fatemeh Azizi[3]

**The development of enzyme-free uric acid (UA) detection methods remains challenging due to cost, stability, and sensitivity limitations. Here, we report a uricase-free colorimetric biosensor using cobalt-1,3,5-benzene tricarboxylate metal–organic frameworks (CoBTC MOFs) with intrinsic peroxidase-like activity. CoBTC catalyzes the oxidation of TMB by conducting $H_2O_2$ to blue oxTMB, while UA reduces oxTMB to colorless TMB, allowing for the quantification of UA via absorbance changes. This biosensor achieved a detection limit of 0.25 µM and a linear range of 0.4–180 µM, outperforming many uricase-dependent assays. Clinical validation with human serum (recovery: 98–103%, RSD < 3%) confirmed the resistance to matrix effects. This work provides a scalable and low-cost alternative for point-of-care UA monitoring in diagnostic settings.**

**Keywords** Enzyme-free, Colorimetric, Uric acid detection, MOF-based nanozyme, Clinical diagnostics

Uric acid, the final product of purine metabolism in humans, is produced primarily in the liver and excreted through the kidneys. This compound plays several roles in the human body, acting as an antioxidant and participating in various biochemical pathways. Uric acid acts as a potent antioxidant to neutralize reactive oxygen species (ROS) and protect cells from oxidative damage. Uric acid is a very important antioxidant that maintains the stability of blood pressure[1]. To date, its dual role as a protective factor and a potential factor in disease has been the subject of extensive research. For example, while it reduces oxidative stress, excessive accumulation of uric acid can lead to the formation of urate crystals, stimulating inflammatory responses and contributing to conditions such as gout. The normal level of uric acid (UA) in serum fluids is 1.5–6 and 2.5–7.0 mg/dL for women and men, respectively[2] and the abnormal level of UA can cause various diseases such as kidney stones, gouty arthritis and hyperuricemia. The global prevalence of hyperuricemia is increasing, making simple and accurate measurement of uric acid levels important for clinical diagnosis and management.

In the past decades, a series of analytical methods have been developed for detecting trace levels of UA, including electrochemical biosensor[3,4], surface-enhanced Raman spectroscopy[5,6], fluorescence spectroscopy[2,7], high performance liquid chromatography[8,9], capillary electrophoresis[10] and colorimetric methods[11]. In recent years, spectrophotometric methods have emerged as promising alternatives for the measurement of uric acid. These methods use colorimetric reactions that result in a measurable absorbance change proportional to the concentration of uric acid. The simplicity and speed of these techniques make them very attractive for routine clinical use. Spectrophotometric methods can be broadly classified into direct and indirect methods. Direct assays rely on the intrinsic absorbance of uric acid, whereas indirect assays involve chemical reactions that produce a measurable color change. Among the indirect methods, the use of chromogenic substrates such as TMB has shown exceptional promise due to their high sensitivity and ease of use.

Enzyme-based colorimetric methods for the detection of UA were first proposed in the early twentieth century[12]. In the presence of uricase, UA can be oxidized to allantoin, producing $H_2O_2$ as a byproduct. Colorimetric methods can directly detect UA or $H_2O_2$ produced from UA oxidation in the presence of uricase. Natural enzymes have high cost of preparation and purification, low stability, and special maintenance and use

[1]Workplace Health Promotion Research Center, Research Institute for Health Sciences and Environment, Shahid Beheshti University of Medical Sciences, Tehran, Iran. [2]Department of Health, Safety, and Environment, School of Public Health and Safety, Shahid Beheshti University of Medical Sciences, Tehran, Iran. [3]Department of Occupational Hygiene Engineering, School of Public Health and Safety, Shahid Beheshti University of Medical Sciences, Tehran, Iran. ✉email: sh_khaloo@sbmu.ac.ir

conditions. Over the past decades, various compounds such as metal–organic frameworks, porphyrins, and metal oxides have been investigated as synthetic enzymes to provide potential alternatives to natural enzymes. Since the discovery of the peroxidase-like catalytic properties of some nanoparticles, there has been a rapid growth in enzyme-like catalytic nanomaterials, known as nanozymes[13]. To date, hundreds of nanozymes have been widely used in sensing, catalysis, and medicine[14]. Peroxidase, oxidase, catalase and superoxide dismutase are four redox enzymes that have been mimicked by nanomaterials in recent years[15]. Recent comprehensive reviews have extensively discussed MOF-based nanozymes and their broad applications. In particular, significant advances have been reported in the use of MOF nanozymes for the detection of mercury ions in environmental samples[16] and for the assay of water-soluble antioxidants and total antioxidant capacity, describing their basic principles and practical applications[17]. These reviews provide valuable background and support for the development of CoBTC-based MOF nanozymes as effective colorimetric probes for the detection of uric acid.

Metal–organic frameworks (MOFs) have attracted considerable attention in various scientific and industrial fields due to their unique structure, high surface area, and tunability[18]. These materials are formed by the binding of metal ions or metal clusters with organic ligands, resulting in crystalline structures with controlled porosity. The diversity in the choice of metal and ligand allows MOFs to be designed for a wide range of applications. Notable applications include gas storage[19], gas separation[20], sensing[21], drug delivery[22], and catalysis[23]. In the field of sensing, MOFs have emerged as promising materials for the development of highly sensitive and selective sensors due to their ability to selectively adsorb analytes and induce detectable changes in physical or chemical properties[24,25]. These features make MOFs an ideal choice for applications such as biosensing and clinical monitoring.

In this study, a colorimetric method based on the oxidation of TMB (3,3',5,5'-tetramethylbenzidine) by hydrogen peroxide ($H_2O_2$) was developed for the sensitive detection of uric acid in the presence of a new two-dimensional catalyst, 2D MOF-CoBTC. The addition of a cobalt-based metal–organic framework (Co-BTC) significantly enhanced the reaction kinetics, resulting in a more intense blue color in a shorter reaction time. When uric acid is introduced into the system, it leads to a decrease in the intensity of the blue color. This decrease in absorbance, which is proportional to the concentration of uric acid, serves as an analytical signal for the quantification of uric acid. The proposed method provides a simple, rapid, and highly sensitive approach for the detection of uric acid, with potential applications in clinical diagnostics and point-of-care testing. Figure 1 illustrate the schematic of the study.

## Materials and methods

### Chemicals and reagents

All of the materials used in this study, such as 1,2,3-benzenetricarboxylic acid (BTC), $Co(NO_3)_2{\cdot}6H_2O$, N,N-dimethylformamide (DMF), and ethanol, were purchased from Merck (Darmstadt, Germany). 3,3′,5,5′-Tetramethylbenzidine (TMB) and uric acid were supplied by Sigma Aldrich. All chemicals were analytical-grade reagents and were used as received without further purification. Double-distilled water was used for the preparation of solutions. A stock solution of 1000 ppm uric acid was prepared in phosphate buffer (pH = 9.0), and other working solutions were obtained by successive dilution of the stock solution.

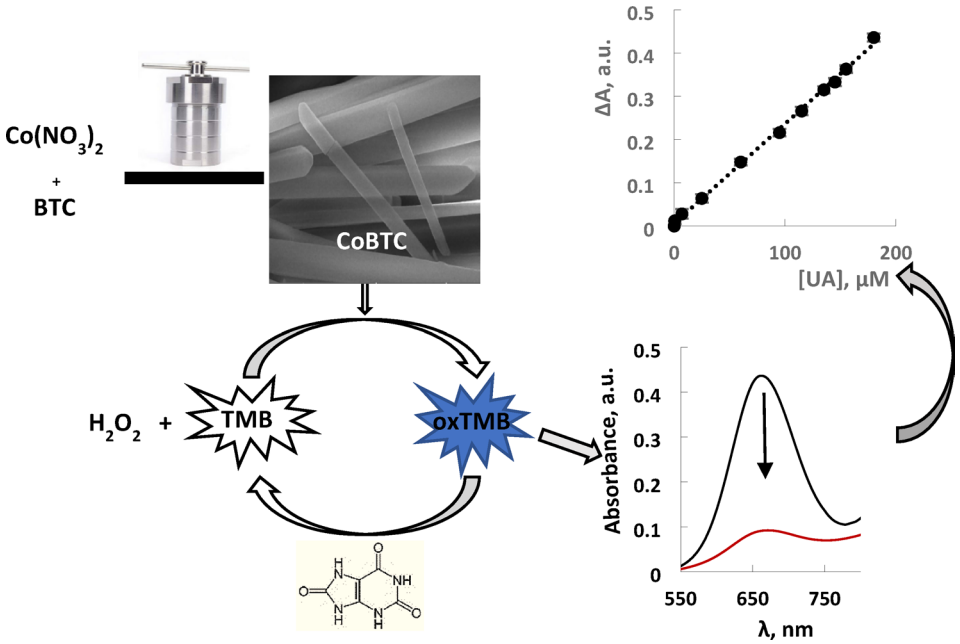


**Fig. 1**. Schematic diagram of the study.

## Synthesis of 2D MOF-CoBTC

The synthesis of the 2D metal–organic framework CoBTC was carried out according to the method described in[23], with minor modifications. A 10 mL solution of $Co(NO_3)_2{\cdot}6H_2O$ (1.16 g) in distilled water with 10 mL of 1,3,5 benzene tricarboxylic acid (BTC, 0.68 g) in N,N-dimethylformamide (DMF) were mixed. The mixture was ultrasonicated for approximately 20 min then the solution was transferred into a 100 ml Teflon-lined stainless-steel autoclave and heated at 135 °C for 12 h. The precipitated purple crystals were collected using centrifugation (5000 rpm for 4 min) and washed with ethanol (3 mL) three times, then rinsed with deionized water twice. The obtained MOF precipitate was dried at 80 °C overnight.

## Instruments

The morphology and elemental analysis of the synthesized CoBTC MOF were assessed using a Czech Republic MIRA3, TESCAN scanning electron microscope equipped with an EDS accessory. The microcrystalline structure of the compounds was analyzed by X-ray diffraction (D8 Advanced Bruker diffractometer) with Cu Kα source radiation within an angle range (2θ) 1–80° operated at 40 kV and 40 mA. FT-IR spectrum of the compounds were recorded at room temperature using KBr method by Agilent, CA, USA spectrometer in the range of 500–4000 $cm^{-1}$. UV–vis spectrum was measured by UV–vis spectrophotometer (AvaSpec-2048, Avantes, Netherlands) at $\lambda_{max}$ according to the experimental condition.

## Pseudo-peroxidase activity of 2D MOF-CoBTC

The pseudo-peroxidase activity of 2D CoBTC was thoroughly investigated using TMB as the substrate and $H_2O_2$ as the oxidant. Prior to kinetic analysis, key experimental parameters such as pH, incubation temperature, $H_2O_2$ concentration, and Co-BTC dosage were optimized to maximize the catalytic efficiency of the catalyst. For example, to study the effect of pH, 200.0 µL of $H_2O_2$ stock solution (10.0 mM), 70.0 µL of TMB stock solution (10.0 mM), and 50.0 µL of 2D Co-BTC suspension (10.0 mg/mL) were mixed in 1680.0 µL of acetate buffer (0.1 M) adjusted to pH values of 3.0, 4.0, 5.0, 6.0, and 7.0. It is worth mentioning that the concentrations in parentheses indicate the initial concentrations of the stock solutions before mixing. The mixture was incubated at 30 °C for 5 min, after which the absorbance was measured at the λ_max using a UV–vis spectrophotometer. Similarly, under the optimized condition of pH 4.0, the effects of temperature (25, 30, 35, 40, and 50 °C), varying MOF dosages (0.1, 0.2, 0.3, 0.4, 0.5, and 0.6 mg/mL), and different $H_2O_2$ concentrations (0.2, 0.5, 0.8, 1, 2, 3, and 5 mM) on the reaction system were studied. These optimizations were performed in a one-factor-at-a-time manner. The concentrations in parentheses in this context represent the final concentrations in the reaction mixture.

To conduct kinetic analysis, the peroxidase-like activity of the 2D Co-BTC was evaluated by varying the concentrations of $H_2O_2$ and TMB under optimal conditions. Specifically, 200.0 µL of $H_2O_2$ stock solution (initial concentration 10.0 mM) was mixed with 70.0 µL of TMB to obtain final TMB concentrations in the range of 0.1 to 1.2 mM, or 70.0 µL of TMB stock solution (10.0 mM) was mixed with 200.0 µL of $H_2O_2$ to obtain final $H_2O_2$ concentrations in the range of 0.1 to 1.5 mM. These solutions were added to acetate buffer (0.1 M, pH 4.0) to a final volume of 1680.0 µL. After that, 50.0 µL of Co-BTC solution (10.0 mg/mL) was added and the mixture was incubated for 5 min at 30°C. The absorbance was then recorded using a UV–vis spectrophotometer at a wavelength of 663 nm. The enzymatic parameters, ($K_m$, Michaelis constant) and ($V_{max}$, maximum reaction rate), for each substrate were calculated using the Michaelis–Menten equation and the Lineweaver–Burk reciprocal equation:

$$\frac{1}{V} = \frac{K_m}{V_{max}} \cdot \frac{1}{[S]} + \frac{1}{V_{max}} \tag{1}$$

Here, V represents the reaction rate and [S] is the substrate concentration.

## Colorimetric determination of Uric acid

For UA colorimetric detection, 200.0 µL of $H_2O_2$ stock solution (10.0 mM), 70.0 µL of TMB stock solution (10.0 mM), and 50.0 µL of 2D Co-BTC suspension (10.0 mg/mL) were mixed in 1580.0 µL of acetate buffer pH 4.0 and 100.0 µL of UA solution with a certain concentration were mixed, shaken and incubated at 30 °C, 5 min. Then, the solution was filtered with a syringe filter (0.45 µm) and monitored using a UV – vis spectrometer at 663 nm. The reduction in absorbance of the solution, in comparison to the blank solution (which contains no uric acid), served as the analytical signal.

To assess the selectivity of the proposed method for uric acid (UA) determination, we prepared various potential interfering substances commonly found in real samples. These included ascorbic acid (AA), urea, glucose (Glu), cysteine (Cys), as well as ions like $Mg^{2+}$, $Ca^{2+}$, $NH_4^+$, $Na^+$, $Cl^-$, $Fe^{2+}$, $Cu^{2+}$, and $K^+$. The absorbance of the solution in the presence of both UA and the interfering substances was followed.

For UA determination in human fluids (serum and urine), samples were first centrifuged at 6000 rpm for 10 min to remove protein species. The supernatants were then diluted, 20-fold for serum and 40-fold for urine, using 0.1 M acetate buffer (pH 4.0) and the UA detection carried out as previously described. The use of human serum and urine samples was approved by the institutional ethics committee affiliated with the hospital (approval number withheld for confidentiality). Informed consent was obtained from all subjects and/or their legal guardians by the hospital at the time of sample collection. All methods were carried out in accordance with relevant guidelines and regulations.

## Results and discussion

### Characterization of MOF-CoBTC

The CoBTC framework contains $Co^{2+}$ cations as central nodes, which are connected through carboxylate groups of benzene carboxylic acid (BTC) ligands[26]. The anisotropic growth of Co-MOF can lead to the formation of nanosheet-like crystals. As shown in Fig. 2a, the scanning electron microscope (SEM) image shows the 2D morphology of the synthesized CoBTC. In addition, elemental composition of the synthesized MOF was determined by energy dispersive spectroscopy (EDS) analysis (Fig. 2b). EDS spectrum confirmed the presence of carbon (C), oxygen (O), and cobalt (Co) atoms in the MOF structure. Also, the elemental mapping (Fig. 2c) results show a uniform distribution of elements on the surface of Co-MOF.

The chemical structure and functional groups of the 2D CoBTC were analyzed using Fourier transform infrared spectroscopy (FTIR), as shown in Fig. 2d. The spectrum showed strong absorption bands corresponding to the symmetric and asymmetric vibrational modes of the carboxylates[26], which were observed in the ranges of 1300–1400 $cm^{-1}$ and 1600–1700 $cm^{-1}$, respectively. Additional bands observed in the 900–1200 $cm^{-1}$ region correspond mainly to C–O stretching vibrations. In addition, several bands identified in the range of 500–800 $cm^{-1}$ were consistent with metal–oxygen (Co–O) interactions[26,27].

To confirm the crystalline structure of cobalt metal–organic framework, the powder X-ray diffraction (XRD) patterns of the synthesized MOF of CoBTC were compared to the simulated pattern of Co-BTC (CCDC: 921,721). As depicted in Fig. 2e, the obtained XRD pattern exhibited sharp diffraction peaks at 2Θ 10.13, 14.65,

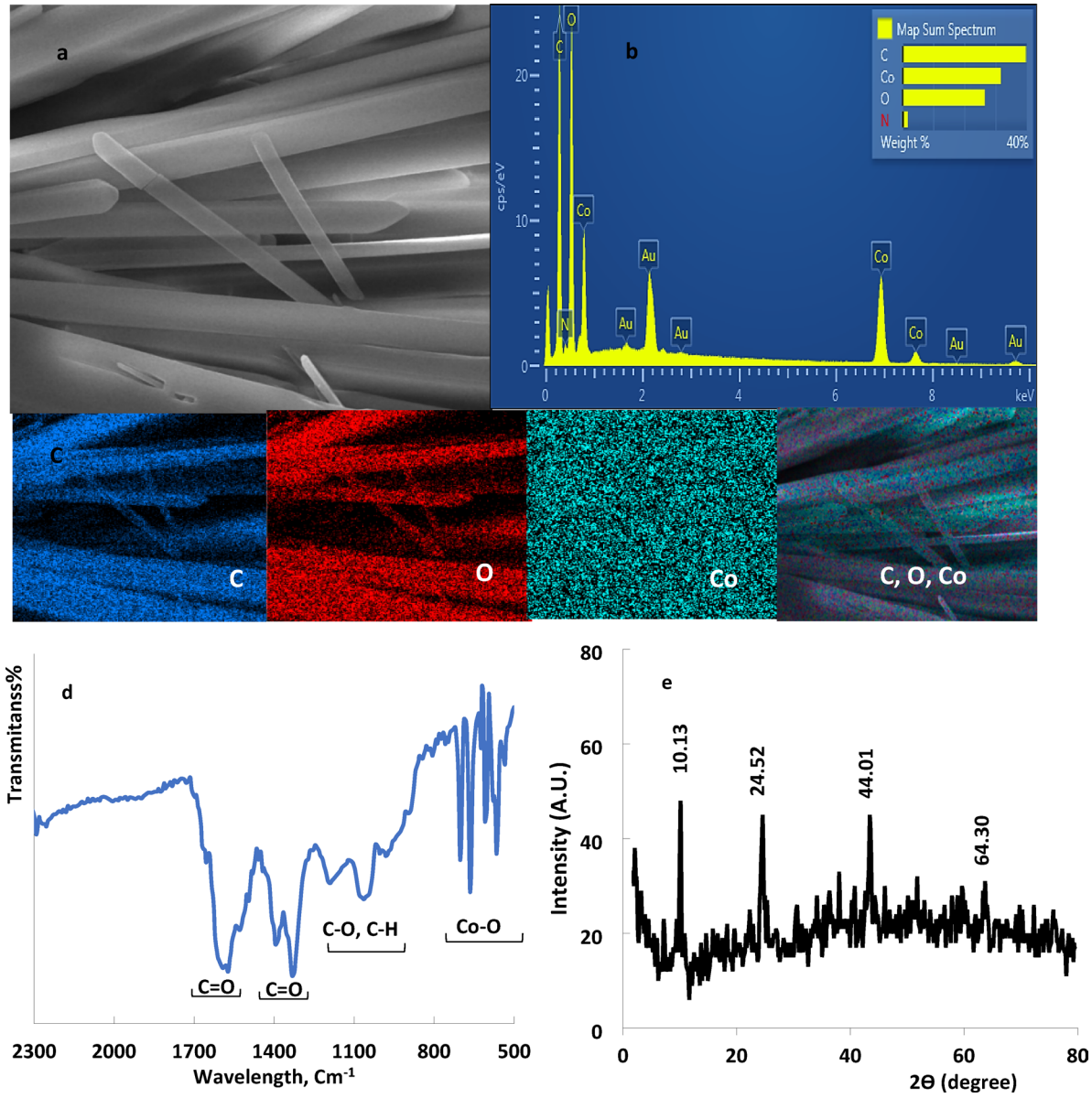


**Fig. 2**. (**a**) SEM micrograph and, (**b**) EDX analysis for the prepared CoBTC and (**c**) the corresponding elemental mapping of CoBTC, (**d**) FT-IR spectrum, and (**e**) X-ray diffraction of CoBTC.

24.52, 44.01, and 64.30 degree that closely matched those of the simulated patterns[28]. The results are in well agreement with ones reported in other literatures[29–31]. In summary, the obtained results confirmed the intrinsic structural features of CoBTC. The synthesized MOF contains two-dimensional thin-layer sheets with uniform thicknesses, high crystallinity structure, and active metal sites, which provide desirable properties for catalysts.

## CoBTC Pseudo-peroxidase activity evaluation

To evaluate the Pseudo-peroxidase activity of the synthesized CoBTC MOF, the catalytic oxidation of TMB, a chromogenic substrate, was investigated in the presence of $H_2O_2$, leading to the formation of a blue-colored product. Figure 3 shows the UV–vis spectra of the reaction systems containing TMB, TMB-$H_2O_2$, TMB-CoBTC, and TMB-CoBTC-$H_2O_2$ in acetate buffer solution (0.1 M, pH 4.0). Notably, TMB alone did not show any absorption at 500–800 nm range (curve a), and this absence of absorption observed even when CoBTC (curve b) or $H_2O_2$ (curve c) were present, indicating that no oxidation reaction had occurred in 5 min. In contrast, a significant absorption peak was observed for the TMB-CoBTC-$H_2O_2$ system (curve d) which reached to its maximum after 5 min. Similar to natural horseradish peroxidase (HRP)[32], CoBTC acts as a peroxidase mimic by providing active sites for electron transfer. The Co(II)/Co(III) redox cycle in the MOF allows for the reduction of hydrogen peroxide to produce reactive oxygen species (ROS), such as hydroxyl radicals ($^{-}OH$) or superoxide radicals ($O^{2-}$). These reactive species act as strong oxidants that catalyze the oxidation of TMB, resulting in the formation of a characteristic blue oxidized product. This redox process mimics the natural enzyme horseradish peroxidase (HRP) but benefits from the stability and reusability of the MOF structure. Such a mechanism is consistent with the general peroxidase-like activity observed in metal–organic frameworks (MOFs) and nanozymes that have been extensively reviewed in the literature[33]. Upon the addition of uric acid to the system, a decrease in the intensity of the blue color is observed (curve e). This decrease in absorbance is directly proportional to the concentration of uric acid, enabling its use as an analytical signal to monitor uric acid levels in various media.

To further elucidate the role of dissolved oxygen in the catalytic mechanism of the synthesized MOF, UV–Vis absorption spectra were recorded under $N_2$-saturated conditions (Fig. 3). Compared with measurements performed in ambient air, the absorption intensity of the oxidized product TMB in $N_2$-saturated solution was significantly reduced. This observation confirms that molecular oxygen is a critical factor in the generation of reactive oxygen species (ROS) via the Co(II)/Co(III) redox cycle. In the absence of sufficient oxygen, the formation of hydroxyl and superoxide radicals is suppressed, leading to a decrease in the catalytic oxidation of TMB.

## Optimization of experimental conditions

The Pseudo-peroxidase activity of CoBTC, similar to other natural catalysts or enzymes, is affected by the reaction conditions. To investigate its potential in biosensor applications, the experimental parameters were optimized before testing with real urea or blood samples. The decrease in absorbance values (ΔA) was used as a signal to optimize it's biosensing performance. Key factors such as pH, temperature, MOF dosage, TMB and $H_2O_2$ concentrations were systematically investigated using a one-factor-at-a-time approach.

pH is a key factor that can significantly enhance or inhibit sensory reactions. The effect of pH on the activity of CoBTC was investigated within the range of 2.0 to 7.0. As illustrated in Fig. 4a, the signal value gradually increases with increasing pH up to 4.0, but decreases with further increase in pH. This behavior can likely be attributed to changes in the surface charge of the catalyst, which may reduce its affinity for the reactants[33]. Consequently, an optimal pH of 4.0 was selected for subsequent experiments.

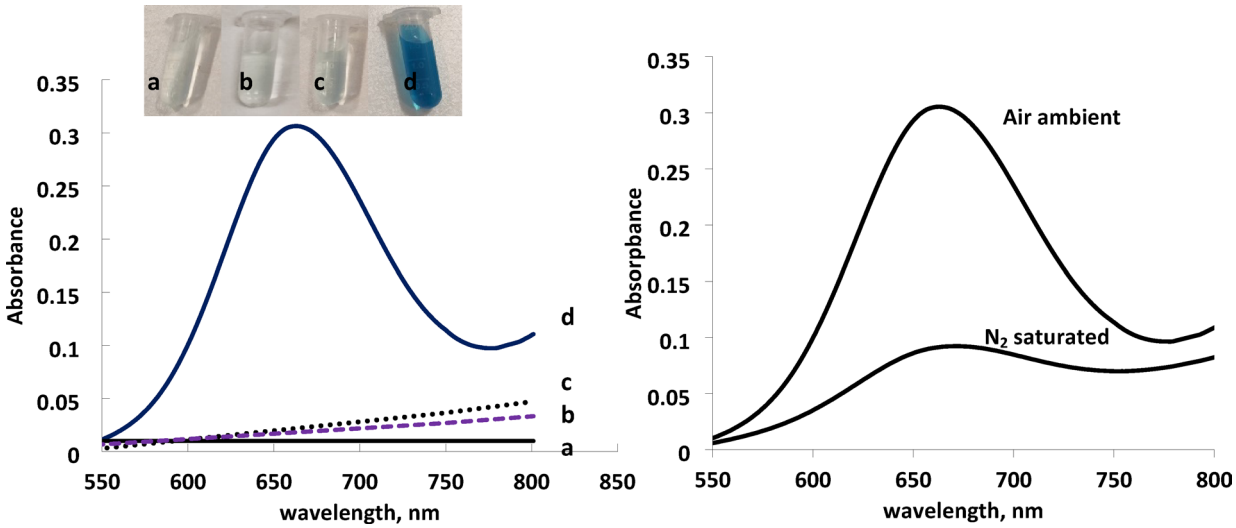


**Fig. 3**. UV–vis spectrum of right (**a**) TMB solution, (**b**) TMB and MOF solution, (**c**) TMB and $H_2O_2$ solution and (**d**) TMB, $H_2O_2$ and CoBTC solution and left UV–vis spectrum of TMB, $H_2O_2$ and CoBTC solution in air ambient and N2 saturated solution.

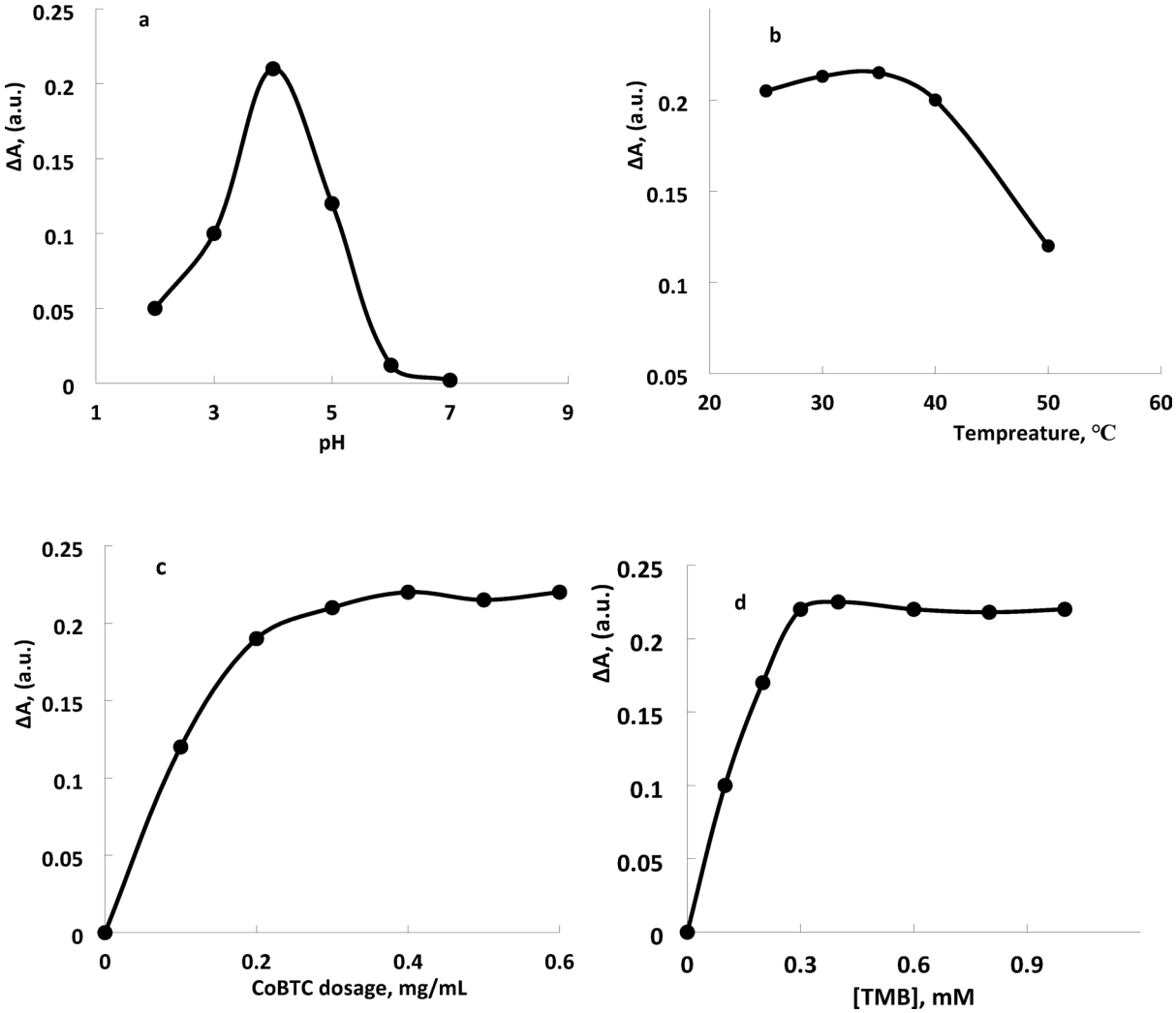


**Fig. 4**. The effect of (**a**) pH, (**b**) Temperature, (**c**) CoBTC dose, and (**d**) TMB concentration on the ΔA.

The effect of temperature on the reaction system was investigated in the range of 25–50 °C (Fig. 4b). The findings showed that there was no significant change in the signal in the temperature range of 25–35 °C. However, increasing the temperature from 35 to 50 °C resulted in a significant decrease in the signal. These results indicated that the catalytic activity of CoBTC produced a significant analytical signal regardless of the temperature, eliminating the need for increasing the temperature. However, further increases in temperature can destroy $H_2O_2$ molecules due to their inherent instability and lead to a decrease in the signal[34,35]. Given that the ambient temperature was 30–32°C, this range was chosen as the optimal value for simplicity.

The effect of the as-synthesized MOF-CoBTC dosage was investigated within the range of 0.2 to 0.6 mg $mL^{-1}$ (Fig. 4c). The signal intensity increases with the catalyst dosage up to 0.3 mg $mL^{-1}$, beyond which it gradually flattened. These results indicate that the activity of the system is highly dependent on the dosage of CoBTC, which must be carefully controlled. Consequently, a dosage of 0.3 mg $mL^{-1}$ was selected for subsequent assays.

TMB is a chromogenic agent and plays a key role in the proposed biosensing of uric acid. Its concentration can directly affect the activity of the system. Therefore, the effect of TMB concentration (0.1–1.0 mM) was investigated (Fig. 4d). It was observed that the analytical signal increased with increasing TMB concentration, then plateaued at concentrations above 350 µM. Consequently, 350 µM was chosen as the optimal TMB concentration. Furthermore, the activity of CoBTC in response to $H_2O_2$ concentration was also studied and the results confirmed that the best peroxidase-like activity was obtained at 100 µM (results not shown).

## Quantitative determination of UA

After optimizing the reaction conditions, a novel enzyme-free biosensor was proposed for the colorimetric assay of uric acid (UA). This approach is based on inhibiting the oxidation of TMB and reducing the intensity of the blue color formed by UA in the presence of CoBTC and $H_2O_2$. As shown in Fig. 5a, with increasing UA concentration, the absorption peak at 663 nm decreases and the dark blue color fades to light blue and finally becomes colorless. This color change can be easily observed with the naked eye. Therefore, the absorbance change of oxidized TMB (oxTMB) was used for the quantitative detection of UA.

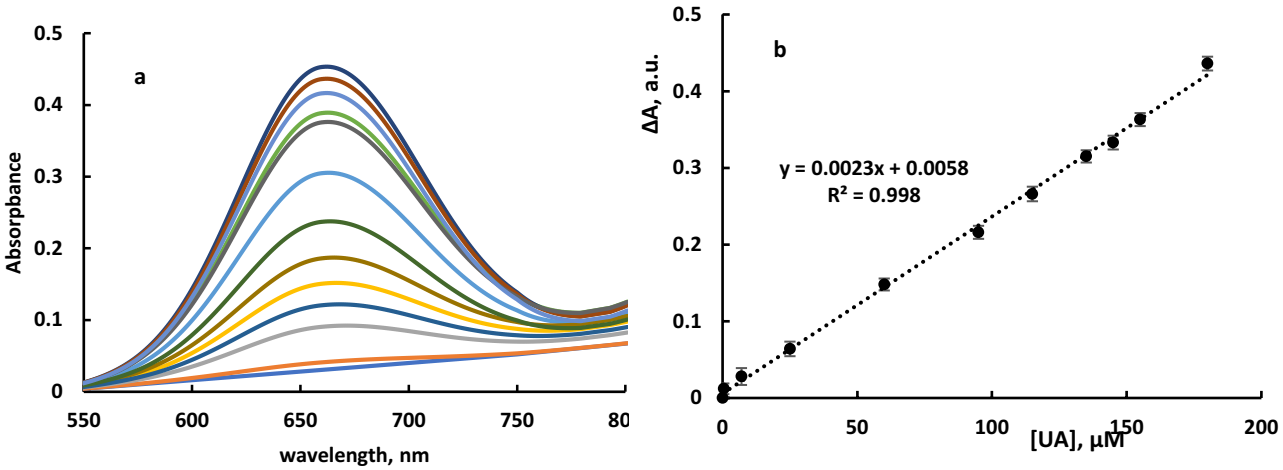


**Fig. 5**. (**a**) UV – vis spectra of the CoBTC biosensor in the presence of different UA concentration (up to down: 0, 0.4, 7, 25, 35, 60, 95, 115, 135, 145,155, 180, and 200 μM). (**b**) Response curve of the ΔA signal as a function of UA concentration (Error bars representing standard deviations from three repeated measurements).

| Material | LOD (μM) | Linear range (μM) | Refrence |
|---|---|---|---|
| silver oxide- activated carbon ionic liquid | 0.000207 | 0.001–0.36 | 36 |
| Pt@Ag nanoflowers | 0.3 | 0.5–150 | 37 |
| $MnO_2$ nanosheets | 0.21 | 0.5–30.0 | 11 |
| AgNPs@MCA* | 0.25 | 0.5–100 | 38 |
| Ionic Liquid-Nickel Nanostructures | 0.13 | 1.0–2.4 | 34 |
| Ni thin film | 3.3 | 15–500 | 39 |
| $Cu_2O$@Au | 0.18 | 0.5–120 | 40 |
| 2D MOF-CoBTC | 0.25 | 0.4–180 | This work |

**Table 1**. Comparative analysis of the colorimetric biosensor for uric acid detection. * Silver nanoparticles modified with 1-methyl-1H-imidazole-2-carbaldehyde.

The dose–response curve of UA was defined by evaluating ΔA (ΔA = $A_0$-A), where $A_0$ represents the absorbance of oxTMB at 663 nm under optimal conditions in the absence of UA (blank solution), and A represents the absorbance of the same solution with different concentrations of UA. As shown (Fig. 5b), the analytical signal gradually increases with increasing UA concentration, and a linear regression curve was obtained for UA concentrations up to 180.0 μM. The results indicate a strong dependence of ΔA on UA level in the range of 0.40–180.0 μM. The linear regression curve can be expressed as $\Delta A = 0.0023[UA] + 0.0059$ ($R^2 = 0.9977$), indicating a sensitivity of 0.0023 $\mu M^{-1}$, which is superior or comparable to other reported sensors (Table 1). The limit of detection (LOD, calculated as 3σ/slope) was determined to be 0.25 μM, which is comparable to or even better than many reported values (Table 1).

The repeatability of the method was assessed through five repeated measurements of a solution containing 50 μM UA, yielding the relative standard deviation (RSD) of 1.03%.

## Steady-state kinetics study

The peroxidase-like activity of CoBTC in the oxidation of TMB was investigated using steady-state kinetics. Kinetic data were collected by fixing the concentration of $H_2O_2$ and changing the concentration of TMB or vice versa. The rate of OxTMB formation was determined by monitoring the increase in absorbance at 663 nm. Figure 6a shows that the rate of the CoBTC peroxidase reaction gradually increased with increasing $H_2O_2$ concentration when TMB was kept constant. However, as $H_2O_2$ reached a certain level, the rate of increase slowed down and finally plateaued.

Similarly, when the concentration of $H_2O_2$ was fixed, the rate of the CoBTC peroxidase reaction increased with higher concentrations of TMB (Fig. 6b). However, beyond a certain concentration of TMB, the reaction rate began to flatten. The kinetic data were analyzed using the Lineweaver–Burk model to fit the Michaelis curve, which resulted in straight lines, as shown in Fig. 6c and d. From the intercepts and slopes of these lines, the kinetic parameters $K_m$ and $V_{max}$ for the MOF-CoBTC catalyst were calculated.

The $K_m$ value, a characteristic constant of enzymes, indicates the affinity between the enzyme and its substrate. A higher $K_m$ indicates a lower affinity. The results showed that the $K_m$ value of CoBTC for TMB and

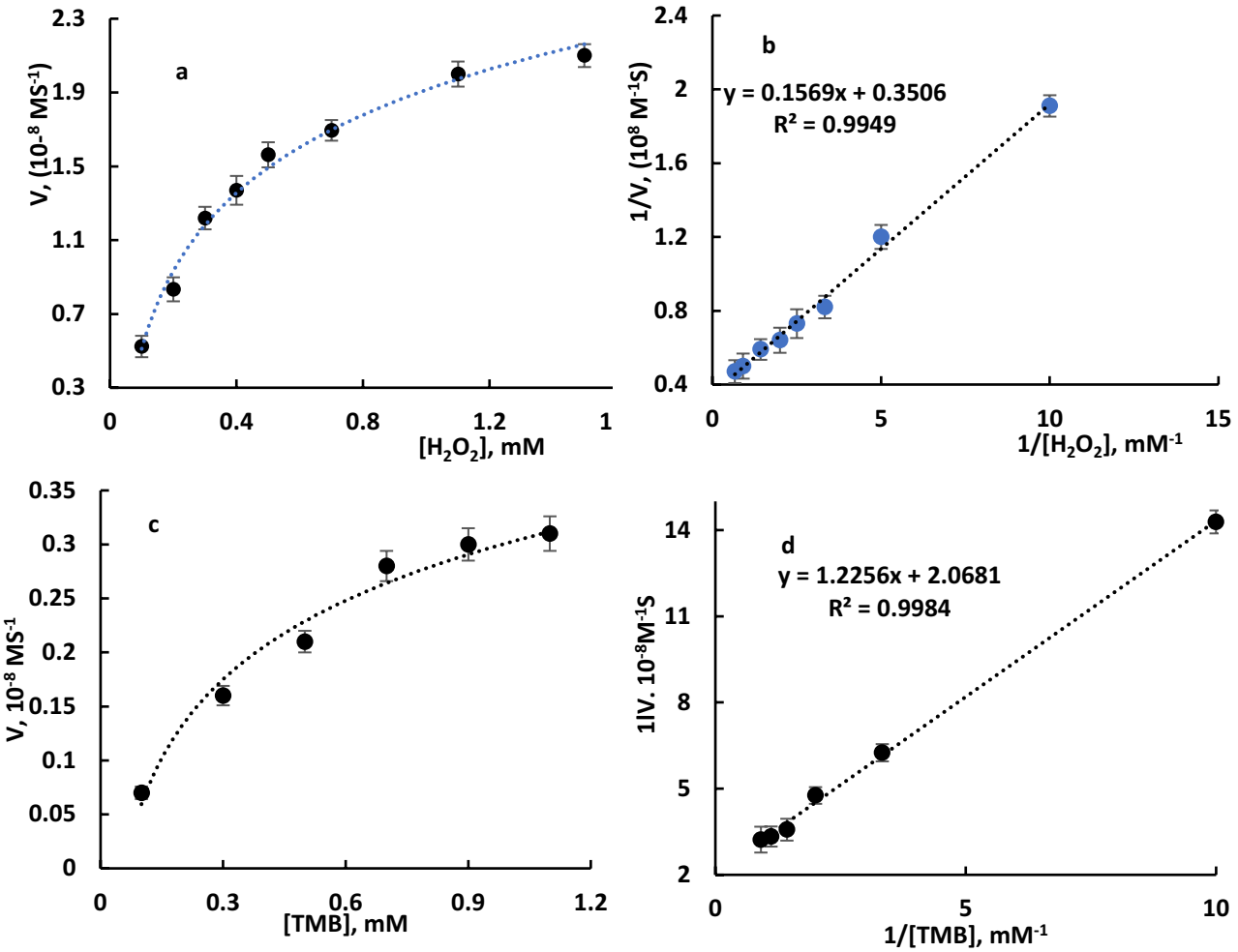


**Fig. 6**. The steady-state kinetic of CoBTC in detection of UA. (**a**) Velocity vs. different concentration of TMB in presence of $H_2O_2$ 1.0 mM. (**b**) Velocity vs. different concentration of $H_2O_2$ in presence of TMB 0.35 mM. and (**c**, **d**) are the corresponding Lineweaver–Burk model (Error bars representing standard deviations from three repeated measurements).

$H_2O_2$ were 0.59 and 0.45 mM, respectively. The $K_m$ value of natural HRP for TMB and $H_2O_2$ are 0.43 and 3.7 mM, respectively[41]. The $K_m$ value of CoBTC for TMB is higher than that of HRP, indicating that CoBTC has a lower affinity for TMB compared to HRP. In contrast, the $K_m$ value of the catalyst for $H_2O_2$ is lower than that of HRP, indicating that CoBTC has a higher affinity for $H_2O_2$, indicating its potential as a synthetic peroxidase.

To evaluate the catalytic efficiency of the synthesized Co-MOF nanozyme, its kinetic parameters (Km and Vmax) were determined for both TMB and $H_2O_2$ substrates and compared with the reported values for other nanozyme-based uric acid sensors as well as the natural enzyme. As summarized in Table 2, the Km and Vmax values of our catalyst fall within the average range among similar systems, indicating moderate substrate affinity and reaction rate, respectively. These findings demonstrate the balanced performance of our Co-MOF nanozyme and make it a promising candidate for practical biosensing applications.

## Interference evaluation and sensing stability

To evaluate the selectivity of the developed UA colorimetric biosensor, this study was conducted under the optimized conditions using various substrates commonly found in blood and urine, including ascorbic acid (AA), urea, triglyceride (Trig), cholesterol (Chol), glucose (Glu), $Mg^{2+}$, $Ca^{2+}$, $Cl^-$, $K^+$, $Na^+$ and $NH_4^+$. The interference study was performed in the presence of 50 µM UA and 50 µM of each of the above compounds. As shown in Fig. 7, the analytical signal (ΔA at 663 nm) shows unsignificant change for UA in presence or absence of other interfering substances, indicating good selectivity for the colorimetric assay of UA. The results confirm that the presence of these interfering compounds does not significantly affect the detection of UA. Therefore, the proposed biosensor exhibits reasonable selectivity, making it suitable for reliable UA assay in blood and urine samples.

The long-term storage stability and reproducibility of the MOF were evaluated under different conditions. The sensor retained more than (98 ± 1.6) % of its initial response after 14 days of storage at room temperature,

| Catalyst | $K_m$ (mM) | | $V_{max}$ ($\mu M.S^{-1}$) | | References |
|---|---|---|---|---|---|
| | $H_2O_2$ | TMB | $H_2O_2$ | TMB | |
| HRP | 3.70 | 0.43 | 0.087 | 0.100 | [41] |
| ZIF-L-Co nanozyme (2D Co-MOF) | 0.48 | 0.52 | 0.022 | 0.035 | [42] |
| Cu-doped biochar nanozyme | 0.42 | 0.60 | 0.031 | 0.033 | [43] |
| Au@Pt nanozyme | 0.20 | 0.25 | 0.028 | 0.031 | [41] |
| $Fe_3O_4$@ZIF-8 nanozyme | 0.28 | 0.25 | 0.025 | 0.027 | [44] |
| CoBTC-MOF nanozyme | 0.45 | 0.59 | 0.022 | 0.032 | This study |

**Table 2**. Comparison of kinetic parameters for nanozyme-based uric acid sensors using TMB and $H_2O_2$

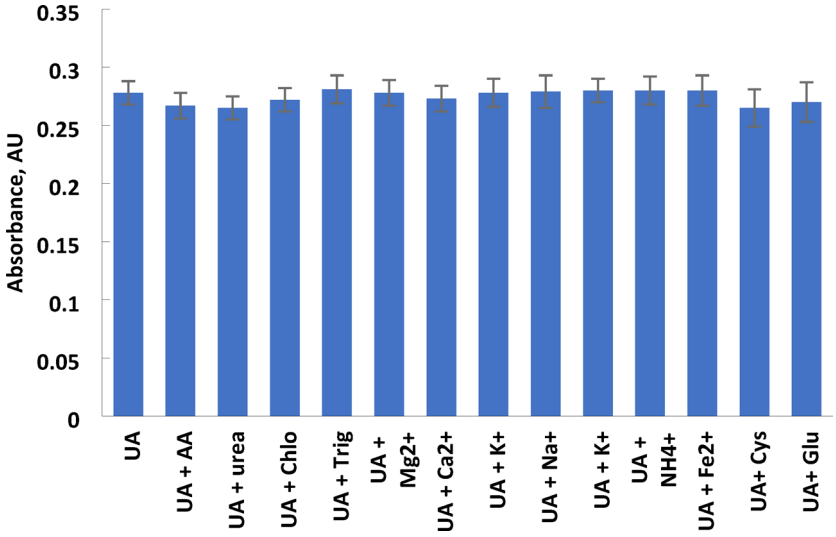


**Fig. 7**. Selectivity of the CoBTC biosensor for UA detection (Error bars representing standard deviations from three repeated measurements).

| Sample | Added (μM) | Measured (μM) | Clinical value (μM) | %Recovery | %RSD |
|---|---|---|---|---|---|
| Serum | Unspiked | 15.63 ± 0.52 | 15.01 | | 3.35 |
| | 30.0 | 44.71 ± 1.21 | | 98.0 | 2.71 |
| | 50.0 | 65.30 ± 0.95 | | 99.5 | 1.45 |
| Urine 1 | Unspiked | 22.45 ± 0.55 | 23.12 | | 2.47 |
| | 30.0 | 52.92 ± 1.16 | | 100.9 | 2.21 |
| | 50.0 | 72.30 ± 1.33 | | 99.8 | 1.85 |
| Urine 2 | Unspiked | 38.56 ± 0.63 | 39.92 | | 1.63 |
| | 30.0 | 70.13 ± 1.06 | | 102.3 | 1.52 |
| | 50.0 | 89.53 ± 1.21 | | 101.1 | 1.35 |

**Table 3**. UA measurements in serum and urine samples using the CoBTC colorimetric sensor.

indicating good retention of catalytic activity under ambient conditions. Also, five replicate measurements of uric acid at a constant concentration showed a relative standard deviation (RSD) of 2.3%, indicating excellent reproducibility. These results demonstrate the successful practical application of the sensor.

## Analysis of human urine and serum samples

To evaluate the feasibility and practical application of the fabricated UA sensor, one human serum sample and two urine samples—originally collected by a hospital for clinical purposes—were analyzed using the proposed method. The results obtained from our biosensor, summarized in Table 3, are comparable to clinical findings. For all samples, the data obtained from our biosensor showed excellent agreement with clinical data, and an average relative error (RE) of 3.47% was obtained. This indicates the high reliability of the proposed biosensor for the measurement of UA in human serum and urine samples. Furthermore, the accuracy of the sensor was

investigated by spiking serum and urine samples with UA standard solutions at different concentrations (30 and 50 μM). The recovery values ranged from 98.0 to 102.3%, with a relative standard deviation (RSD) range of 1.35–3.35%. These satisfactory results confirmed the feasibility and good reproducibility of the developed colorimetric sensor during practical sample measurements.

## Conclusion

In summary, a novel 2D CoBTC nanozyme was developed, which exhibited significantly enhanced pseudo-peroxidase activity due to its catalytic effect on TMB oxidation in the presence of $H_2O_2$. Interestingly, it was observed that the TMB color reaction could be inhibited by UA, and make a visible color change detectable by the naked eye. Taking advantage of this phenomenon, a novel enzyme-free UA colorimetric biosensor was successfully developed. This biosensor exhibits excellent reproducibility and environmental stability. Under optimized conditions, a strong linear relationship between ΔA and UA concentration was observed in the range of 0.4–180.0 μM, with a limit of detection (LOD) of 0.25 μM. Importantly, the fabricated biosensor shows promising potential for UA detection in real human samples. These advantages collectively position the developed biosensor as a simple, reliable, and promising tool for UA assay in clinical diagnostics and bioanalysis.

## Data availability

The datasets generated and/or analysed during the current study are available from the corresponding author on reasonable request.

Received: 31 May 2025; Accepted: 3 November 2025
Published online: 05 December 2025

## References

1. Wang, Q., Wen, X. & Kong, J. Recent progress on uric acid detection: A review. *Crit. Rev. Anal. Chem.* **50**(4), 359–375 (2020).
2. Zheng, X. et al. Enzyme-free fluorescence determination of uric acid by combining CdTe quantum dots with metal–organic framework for signal amplification. *Microchim. Acta* **189**(11), 435 (2022).
3. Yan, Q. et al. A highly sensitive uric acid electrochemical biosensor based on a nano-cube cuprous oxide/ferrocene/uricase modified glassy carbon electrode. *Sci. Rep.* **10**(1), 10607 (2020).
4. Nazir, A. et al. A flexible carbon nanotubes-based microelectrode for non-enzymatic electrochemical uric acid and ascorbic acid sensing. *Mater. Sci. Eng., B* **307**, 117480 (2024).
5. Zhou, J.-W. et al. Reliable quantitative detection of uric acid in urine by surface-enhanced Raman spectroscopy with endogenous internal standard. *Biosens. Bioelectron.* **251**, 116101 (2024).
6. Li, J. et al. Quantification of uric acid concentration in tears by using PDMS inverse opal structure surface-enhanced Raman scattering substrates: Application in hyperuricemia. *Spectrochim. Acta Part A Mol. Biomol. Spectrosc.* **278**, 121326 (2022).
7. Li, F. et al. Ratiometric fluorescence and colorimetric detection for uric acid using bifunctional carbon dots. *Sens. Actuators, B Chem.* **369**, 132381 (2022).
8. Wu, M. et al. Simultaneous determination of purines and uric acid in chinese chicken broth using TFA/FA hydrolysis coupled with HPLC-VWD. *Foods* **10**(11), 2814 (2021).
9. Das, L. et al. Validation and comparison of analytical methods for the determination of uric acid in pulses and cereals by salting out assisted extraction by Rapid resolution liquid chromatography. *J. Chromatogr. B* **1180**, 122894 (2021).
10. Moravčík, O., Dvořák, M. & Kubáň, P. Autonomous capillary electrophoresis processing and analysis of dried blood spots for high-throughput determination of uric acid. *Anal. Chim. Acta* **1267**, 341390 (2023).
11. Huang, L. et al. Enzyme-free colorimetric detection of uric acid on the basis of $MnO_2$ nanosheets–mediated oxidation of 3, 3′, 5, 5′- tetramethylbenzidine. *Microchem. J.* **190**, 108719 (2023).
12. Neilans, G. A. E. P. The determination of uric acid in biological material. *J. Biol. Chem.* **69**(2), 427–433 (1926).
13. Manea, F. et al. Nanozymes: Gold-nanoparticle-based transphosphorylation catalysts. *Angew. Chem. Int. Ed.* **43**(45), 6165–6169 (2004).
14. Zandieh, M. & Liu, J. Nanozymes: Definition, activity, and mechanisms. *Adv. Mater.* **36**(10), 2211041 (2024).
15. Yuan, X. et al. Advances in nanozymes with peroxidase-like activity for biosensing and disease therapy applications. *J. Mater. Chem. B* **13**(5), 1599–1618 (2025).
16. Mohammed Ameen, S. S. et al. Recent advances of metal-organic frameworks as nanozymes for mercury ions detection in environmental samples. *Mater. Today Chem.* **45**, 102686 (2025).
17. Ameen, S. S. M. & Omer, K. M. Metal-organic framework-based nanozymes for water-soluble antioxidants and total antioxidant capacity detection: Principles and applications. *Food Chem.* **479**, 143876 (2025).
18. Laeim, H. et al. Porosity tunable metal-organic framework (MOF)-based composites for energy storage applications: Recent progress. *Polymers* **17**(2), 130 (2025).
19. Heinz, K. et al. MOFs for long-term gas storage: Exploiting kinetic trapping in ZIF-8 for on-demand and stimuli-controlled gas release. *Inorg. Chem. Front.* **10**(16), 4763–4772 (2023).
20. Ge, C. et al. Pore-optimized MOF-808 made through a facile method using for fabrication of high-performance mixed matrix composite $CO_2$ capture membranes. *Carbon Capture Sci. Technol.* **10**, 100156 (2024).
21. Sohrabi, H. et al. Metal-organic frameworks (MOF)-based sensors for detection of toxic gases: A review of current status and future prospects. *Mater. Chem. Phys.* **299**, 127512 (2023).
22. Pederneira, N. et al. Drug delivery on Mg-MOF-74: The effect of drug solubility on pharmacokinetics. *ACS Appl. Bio. Mater.* **6**(6), 2477–2486 (2023).
23. Yaqoob, L. et al. Nanocomposites of cobalt benzene tricarboxylic acid MOF with rGO: An efficient and robust electrocatalyst for oxygen evolution reaction (OER). *Renew. Energy* **156**, 1040–1054 (2020).
24. Kumar, R. et al. Recent advances in MOF-based materials for biosensing applications. *Sensors* **25**(8), 2473 (2025).
25. Quan, Y. et al. Metal–organic framework-based SERS probes with enrichment capability for trace detection: Applications in biomarkers and pollutants. *Microchim. Acta* **192**(3), 200 (2025).
26. Al Lawati, H. A. J. & Hassanzadeh, J. Dual-function 2D cobalt metal-organic framework embedded on paper as a point-of-care diagnostic device: Application for the quantification of glucose. *Anal. Chimica Acta* **1139**, 15–26 (2020).
27. Yao, W. et al. Synthesis, structure, adsorption and electrochemical properties of the new two-dimensional cobalt coordination polymer based on bifunctional ligand. *Trans. Met. Chem.* **49**(5), 331–341 (2024).
28. Irandoost, E. et al. Cobalt–organic framework as a Bi–functional electrocatalyst for renewable hydrogen production by electrochemical water splitting. *Appl. Energy nd Combust. Sci.* **17**, 100240 (2024).

29. Vinoth Kumar, R. et al. Cobalt phosphate-benzene-1,3,5-tricarboxylic acid metal–organic framework @ reduced graphene oxide electrodes for hybrid supercapacitors. *J. Mater. Sci.* **59**(13), 5498–5517 (2024).
30. Arjmand, F. & Ranjbar, Z. Impact of copper and cobalt-based metal-organic framework materials on the performance and stability of hole-transfer layer (HTL)-free perovskite solar cells and carbon-based. *Sci. Rep.* **14**(1), 12843 (2024).
31. Ethiraj, J. et al. Water-driven structural transformation in cobalt trimesate metal-organic frameworks. *Energies* **14**(16), 4751 (2021).
32. Yu, H. et al. A nano-sized Cu-MOF with high peroxidase-like activity and its potential application in colorimetric detection of $H_2O_2$ and glucose. *RSC Adv.* **11**(43), 26963–26973 (2021).
33. Kong, X.-J. et al. Reversible Co(II)–Co(III) transformation in a family of metal-dipyrazolate frameworks. *J. Am. Chem. Soc.* **146**(41), 28320–28328 (2024).
34. Nishan, U. et al. Development of a nonenzymatic colorimetric sensor for the detection of uric acid based on ionic liquid-mediated nickel nanostructures. *ACS Omega* **7**(30), 26983–26991 (2022).
35. Chen, X. et al. Nanozyme's catalytic activity at neutral pH: Reaction substrates and application in sensing. *Anal. Bioanal. Chem.* **415**(18), 3817–3830 (2023).
36. Nishan, U. et al. Uric acid quantification via colorimetric detection utilizing silver oxide-modified activated carbon nanoparticles functionalized with ionic liquid. *RSC Adv.* **14**(10), 7022–7030 (2024).
37. Wang, X. et al. Ultrasensitive detection of uric acid in serum of patients with gout by a new assay based on Pt@Ag nanoflowers. *RSC Adv.* **9**(63), 36578–36585 (2019).
38. DongboYang, et al. A simple and rapid colorimetric sensor for uric acid detection based on ligand-modified silver nanoparticles with oxidase activity. *Microchim. Acta* **192**(10), 695 (2025).
39. Tripathi, A., Harris, K. D. & Elias, A. L. Peroxidase-like behavior of Ni thin films deposited by glancing angle deposition for enzyme-free uric acid sensing. *ACS Omega* **5**(16), 9123–9130 (2020).
40. Liang, D. et al. Dual model biosensor integrated with peroxidase-like activity and self-assembly for uric acid detection. *J. Mater. Chem. B* **13**(24), 7146–7154 (2025).
41. Panferov, V. G., Wang, X. & Liu, J. Characterization of nanozyme kinetics for highly sensitive detection. *Analyst* **149**(8), 2223–2226 (2024).
42. Sethi, S. & Rathod, V. K. Rapid multi-mode optical colorimetric detection of $H_2O_2$, uric acid, and dopamine using cobalt-based 2D ZIF-L-Co nanozyme. *BioNanoScience* **15**(3), 449 (2025).
43. Khan, N. et al. Optical detection of uric acid based on a citric acid functionalized copper-doped biochar nanozyme. *RSC Adv.* **14**(45), 33007–33018 (2024).
44. Ke, W. et al. Enzyme cascade nanozyme based colorimetric sensor for detection of uric acid as a biomarker of hyperuricemia. *Microchim. Acta* **192**(2), 85 (2025).


## Acknowledgements

The authors gratefully acknowledge the financial support of this proposal by the Shahid Beheshti University of Medical Sciences with grant No: 43006286. The authors gratefully acknowledge the support of this work by the Workplace Health Promotion Research Center, Shahid Beheshti University of Medical Sciences, Tehran, Iran.

## Author contributions

S. S. Kh.: Conceptualization, supervision, writing—review and editing manuscript, M. H. V.: review of data analysis, writing—supporting draft, F.A.: performing all experimental work, data analysis.

## Declarations

## Competing interests

The authors declare that they have no known competing financial interests or personal relationships that could have appeared to influence the work reported in this paper.

## Ethical approval and consent to participate

This proposal has the ethical code of IR. SBMU.PHNS. REC.1402.033 from ethical commission of Shahid Beheshti University of Medical Sciences.

## Additional information

**Correspondence** and requests for materials should be addressed to S.S.K.

**Reprints and permissions information** is available at www.nature.com/reprints.

**Publisher's note** Springer Nature remains neutral with regard to jurisdictional claims in published maps and institutional affiliations.